TITLE: The Effects of Anisotropy on Regional Seismic Wave Propagation

PRINCIPAL INVESTIGATOR: Jeffrey Park
Co-WORKERS: Liqiang Su, Jonathan Lilly
AFFILIATION: Department of Geology and Geophysics, Box 208109
Yale University, New Haven, CT 06520-8109
AFOSR contract: F49620-94-1-0043

August 3, 1995

ABSTRACT

We have examined the effect of seismic anisotropy on the scattering of surface waves in actively-deforming continental regions, many of which occur in areas of nonproliferation concern. We have approached the problem from three angles, 1) we have developed waveform inversion methods for Love-Rayleigh coupling in seismic data from the Tibetan Plateau and Tien Shan region, 2) we have developed a flat-layered surface wave code to study the effect of crust and upper-mantle anisotropy on crustal resonances, and 3) we have advanced wavelet-based signal processing methods to estimate the polarization of coherent seismic energy across a broadband seismic array. In data from the recent portable broadband PASSCAL deployment in Tibet, we found clear evidence of long-period Love-to-Rayleigh scattering that is best explained by lateral gradients of anisotropy in the upper mantle, developed in the course of the compression and uplift of the plateau. We developed a modal summation technique for waveform perturbations that allowed us to infer that *both* S and P wave anisotropy, with a ratio consistent with the mineral alignment of sheared peridotite, in the depth range 100–300 km are necessary to fit the observed data. Using a plane-layered geometry, we are investigating the effect of crust and upper mantle anisotropy on Love-Rayleigh coupling in the 5-30 second period range. Most previous studies have posited a horizontal or vertical axis of symmetry for seismic anisotropy, but our code can incorporate a tilted axis of symmetry, which enhances coupling and scattering effects. Such dipping geometries could develop in the crust as a result of thrust ramps in compressive tectonic regimes, either in the form of oriented crystals in shear zones or fine-layering of isotropic material. We have developed a multiple-station wavelet-based method for detecting frequency-dependent polarization in noisy seismic data. The wavelet method, unlike the moving-window Fourier transform, scales the time interval analysed to the period of the presumed signal. We have applied this method successfully thusfar to Terrascope data from Southern California, and have documented a strong refraction of intermediate-period surface waves along the "big-bend" portion of the San Andreas Fault.

OBJECTIVE

We wish to determine the effect of seismic anisotropy, within the crust and uppermost mantle, on surface waves with periods between 10 and 30 seconds. In particular, we wish to characterize the scattering caused by lateral variations in anisotropy in regions of past and present lithospheric deformation. This path-dependent scattering can distort seismic waveforms, and make more difficult the discrimination of explosions from earthquakes. We plan to identify regions of the Earth where scattering associated with lithospheric anisotropy is important. Data from regional networks and arrays located in Eurasia and the US will also be used in experiments to extract 'scattered' waveforms from the principal Love and Rayleigh wavepackets. In addition to standard stacking/beamforming techniques, we will develop a frequency-dependent variant of the MUSIC algorithm to identify coherent surface waves that traverse an array. We plan to test, in selected areas, whether anisotropy inferred from the 'splitting' of 1-20 second shear waves is sufficient to explain observed Love to Rayleigh scattering.

TECHNICAL PROPOSAL: RESEARCH ACCOMPLISHED

We have developed codes for the dispersion characteristics of crustal surface waves in a 1-D anisotropic media, with anisotropy that is hexagonally symmetric, but with an axis of symmetry that is arbitrary. Previous investigators have restricted attention to symmetry axes that are either vertical or horizontal, but a tilted axis of symmetry is plausible in the uppermost crust and perhaps near the Moho, where thrusting and extension involves a combination of vertical and horizontal deformation. A modification of this code can be used to examine the behavior of teleseismic body waves that propagate upward through an anisotropic crustal structure. Enhanced coupling between P-SV and the SH particle motion occurs for waves that have significantly non-vertical incidence, in particular between P and SH motion.

We would like to express the interaction of upgoing and downgoing plane waves in a weakly anisotropic layered medium with hexagonal symmetry. Hexagonal symmetry implies a stress-strain relation that possesses an axis of symmetry $\hat{\mathbf{w}}$. Elastic properties are constant within each of a stack of layers over a uniform halfspace, but the axis of symmetry can vary among the layers. We express the elastic properties as a function of depth as $\Lambda(r)$, where Λ_{ijkl} is the fourth-order stress-strain tensor. If the axis of symmetry is horizontal, we can express the azimuthal dependence of the squared P and SV velocities for horizontal propagation in terms of the angle ξ from $\hat{\mathbf{w}}$, according to formulas similar to the head-wave formulas of *Backus*, [1965], *Crampin* [1977] and *Park* [1993]:

$$\begin{aligned} \rho\alpha^2(\xi) &= A + B\cos 2\xi + C\cos 4\xi \\ \rho\beta^2(\xi) &= D + E\cos 2\xi. \end{aligned} \tag{1}$$

If density perturbations are neglected, knowledge of A, B, C, D, E is sufficient to determine the stress-strain tensor [*Shearer and Orcutt*, 1986]. *Park* [1993] showed how these azimuthal relations generalize to other orientations of $\hat{\mathbf{w}}$. We assume a flat earth, $z = 0$ at the free surface, and z increasing downward. We assume a plane-wave solution of the form $\mathbf{U}(\mathbf{x}, t) =$

$\mathbf{u}(\mathbf{x})e^{i(\mathbf{k}\cdot\mathbf{x}-\omega t)}$. The strain tensor

$$\epsilon = \frac{1}{2}(\nabla\mathbf{u} + (\nabla\mathbf{u})^T) = \frac{i}{2}(\mathbf{k}\otimes\mathbf{u} + \mathbf{u}\otimes\mathbf{k})e^{i(\mathbf{k}\cdot\mathbf{x}-\omega t)}$$

In each layer, the elastic tensor can be expressed

$$\mathbf{\Lambda} = A\mathbf{\Lambda}_A + B\mathbf{\Lambda}_B + C\mathbf{\Lambda}_C + D\mathbf{\Lambda}_D + E\mathbf{\Lambda}_E, \tag{2}$$

where

$$\begin{aligned}
\mathbf{\Lambda}_A &= \mathbf{I}\otimes\mathbf{I} \\
\mathbf{\Lambda}_B &= \mathbf{W}\otimes\mathbf{I} + \mathbf{I}\otimes\mathbf{W} \\
\mathbf{\Lambda}_C &= 8\mathbf{W}\otimes\mathbf{W} - \mathbf{I}\otimes\mathbf{I} \\
\mathbf{\Lambda}_D &= (13)\mathbf{I}\otimes\mathbf{I} + (14)\mathbf{I}\otimes\mathbf{I} - 2\mathbf{I}\otimes\mathbf{I} \\
\mathbf{\Lambda}_E &= 2[(13)\mathbf{\Lambda}_B + (14)\mathbf{\Lambda}_B - 2\mathbf{\Lambda}_B] + \mathbf{\Lambda}_D,
\end{aligned} \tag{3}$$

where '$\otimes$' is the tensor product operation, and $\mathbf{W} = \hat{\mathbf{w}}\otimes\hat{\mathbf{w}} - \frac{1}{2}\mathbf{I}$, where $\mathbf{I}$ is the identity tensor. The permutation (ij) indicates the interchange of the ith and jth tensor index e.g., $\{(13)\mathbf{I}\otimes\mathbf{I}\}_{ijkl} = \delta_{kj}\delta_{il}$. An isotropic elastic tensor $\mathbf{\Lambda}^{(0)}$ contains only terms proportional to the isotropic tensors $\mathbf{\Lambda}_A$ and $\mathbf{\Lambda}_D$, as neither depends on $\hat{\mathbf{w}}$.

Because P, SV and SH motion can couple at all interfaces in a layered anisotropic structure with general axis of symmetry $\hat{\mathbf{w}}$, all interacting upgoing and downgoing plane waves share the same horizontal wavenumber. Let $\frac{\mathbf{k}}{\omega} = p\hat{\mathbf{x}} + \nu\hat{\mathbf{z}}$, where p and ν are the horizontal and vertical slownesses, respectively. In a general anisotropic medium, there are three upgoing and three downgoing plane waves. For fixed p, the Christoffel relations lead to six possible solutions for ν, as determined by the quadratic eigenvalue problem

$$(p^2\mathbf{T} - \rho\mathbf{I} + \nu p\mathbf{S} + \nu^2\mathbf{R})\cdot\mathbf{u} = 0 \tag{4}$$

where

$$\begin{aligned}
\mathbf{T} &= (A - B + C - D + E)\hat{\mathbf{x}}\otimes\hat{\mathbf{x}} + (D + (2w_x^2 - 1)E)\mathbf{I} + (8w_x^2C + 2E)\hat{\mathbf{w}}\otimes\hat{\mathbf{w}} \\
&\quad + (B - 4C - 2E)w_x(\hat{\mathbf{w}}\otimes\hat{\mathbf{x}} + \hat{\mathbf{x}}\otimes\hat{\mathbf{w}}) \\
\mathbf{S} &= (A - B + C - D + E)(\hat{\mathbf{x}}\otimes\hat{\mathbf{z}} + \hat{\mathbf{z}}\otimes\hat{\mathbf{x}}) + 4w_xw_zE\mathbf{I} + 16w_xw_zC\hat{\mathbf{w}}\otimes\hat{\mathbf{w}} \\
&\quad + (B - 4C - 2E)[w_z(\hat{\mathbf{w}}\otimes\hat{\mathbf{x}} + \hat{\mathbf{x}}\otimes\hat{\mathbf{w}}) + w_x(\hat{\mathbf{w}}\otimes\hat{\mathbf{z}} + \hat{\mathbf{z}}\otimes\hat{\mathbf{w}})] \\
\mathbf{R} &= (A - B + C - D + E)\hat{\mathbf{z}}\otimes\hat{\mathbf{z}} + (D + (2w_z^2 - 1)E)\mathbf{I} + (8w_z^2C + 2E)\hat{\mathbf{w}}\otimes\hat{\mathbf{w}} \\
&\quad + (B - 4C - 2E)w_z(\hat{\mathbf{w}}\otimes\hat{\mathbf{z}} + \hat{\mathbf{z}}\otimes\hat{\mathbf{w}})
\end{aligned} \tag{5}$$

To transform (8) into a linear 6×6 eigenproblem, define $\tilde{\mathbf{T}} = \mathbf{R}^{-1}\cdot(p^2\mathbf{T} - \rho\mathbf{I})$ and $\tilde{\mathbf{S}} = p\mathbf{R}^{-1}\cdot\mathbf{S}$ to obtain $(\tilde{\mathbf{T}} + \nu\tilde{\mathbf{S}} + \nu^2\mathbf{I})\cdot\mathbf{u} = 0$. This 3×3 system can be solved with the 6×6 system

$$(\mathcal{T} - \nu\mathcal{I})\cdot\mathcal{U} = \left(\begin{bmatrix} -\tilde{\mathbf{S}} & -\tilde{\mathbf{T}} \\ \mathbf{I} & 0 \end{bmatrix} - \nu\begin{bmatrix} \mathbf{I} & 0 \\ 0 & \mathbf{I} \end{bmatrix}\right)\cdot\begin{bmatrix} \nu\mathbf{u} \\ \mathbf{u} \end{bmatrix} = 0 \tag{6}$$

Solving (6) will obtain three upgoing and three downgoing waves, aside from exceptional cases e.g., if p equals the P or S slowness in a layer and the associated wave travels horizontally. (In this case the matrix system is formally defective.) To solve the equation of motion

in a stack of constant-property layers, one matches boundary conditions for traction and displacement continuity for these six waves at each interface. We obtain surface-wave modes by forcing an evanescent condition in the halfspace, propagating the stress-displacement vector to the free surface, and enforcing a zero-traction condition. There are several schemes for doing this. We have adapted the computational algorithm of *Chen* [1993], which forces all evanescent waves to "decay" away from interfaces to decrease roundoff error. At a fixed frequency, the algorithm searches the allowable interval of horizontal slowness for roots to the secular function that describes free-surface traction. The computational formulas are quite similar to the Rayleigh-wave formulas of *Chen* [1993], except that the reflection and transmission matrices are 3×3, rather than 2×2. The numerical application is complicated by the need to separate travelling modes that are closely spaced in phase velocity. To keep track of solutions, we use the group velocity of a mode at a frequency f to predict a phase-velocity "window" in which a solution should be found at frequency $f + \delta f$. This also reduces the number of propagator-evaluations of the surface traction condition, each of which requires solution of a 6×6 eigenvector system in each layer. This type of interpolator is not always successful, unfortunately, because the coupling of Rayleigh and Love motion can cause "bow-ties" in the dispersion curves where surface-wave modes mix in near-equal amounts - see Figure 1.

We have developed and coded a path-integral formalism to invert Love-to-Rayleigh and Rayleigh-to-Love scattered waveforms. Although we plan to apply these techniques to flat-layer geometry for crustal/lithospheric surface waves, our earlier work made natural the initial development of a spherical-earth formalism using coupled free oscillations. A problem when calculating coupled-mode synthetics in a 3-D earth model is the sum over all singlets associated with spherical harmonic multiplets. By using the summation theorem of spherical harmonics, we sum the singlets analytically and calculate the synthetics by summing multiplets rather than singlets. We expand the elastic tensor to a general 6×6 matrix to handle arbitrary orientations of the anisotropic fast axis. This technique enables us not only to calculate synthetics quickly in a 3-D anisotropic structure but also to establish an inverse algorithm because of the linear property of differential seismograms. These synthetics compare well with 3-D strong Born synthetics, which implies that, for the models we have considered, Love-Rayleigh scattering occurs primarily along the great-circle path. We use the great-circle technique to fit waveforms recorded in a recent broadband PASSCAL experiment in Tibet (Figure 2). We find that the observed waveform anomalies in the southern part of the Plateau can be well explained with a strong anisotropic gradient zone beneath the central Plateau. An additional anisotropic zone in central Alaska can be used to fit details in the Tibet data better. The presence of such an anisotropic zone is supported by a quasi-Love wave, observed at College, Alaska, in data from the 1/16/95 Kobe, Japan earthquake.

We have also extended the multiple wavelet polarization method to apply to three-component array data. We have been testing this method on data from the Terrascope broadband regional network in Southern California. The wavelet method enables the user to pick apart the time-frequency behavior of seismic data, and the SVD-polarization code enables the user to correlate motion between stations, preserving the small time shifts and amplitude/polarization variability that would be averaged out in simple beamforming. For surface waves in the 40-100 sec period range, there is considerable variability in amplitude and polarization within the roughly 250 km aperture of the Terrascope network. There is also evidence for significant Love-to-Rayleigh forward scattering in the 40-100 sec period

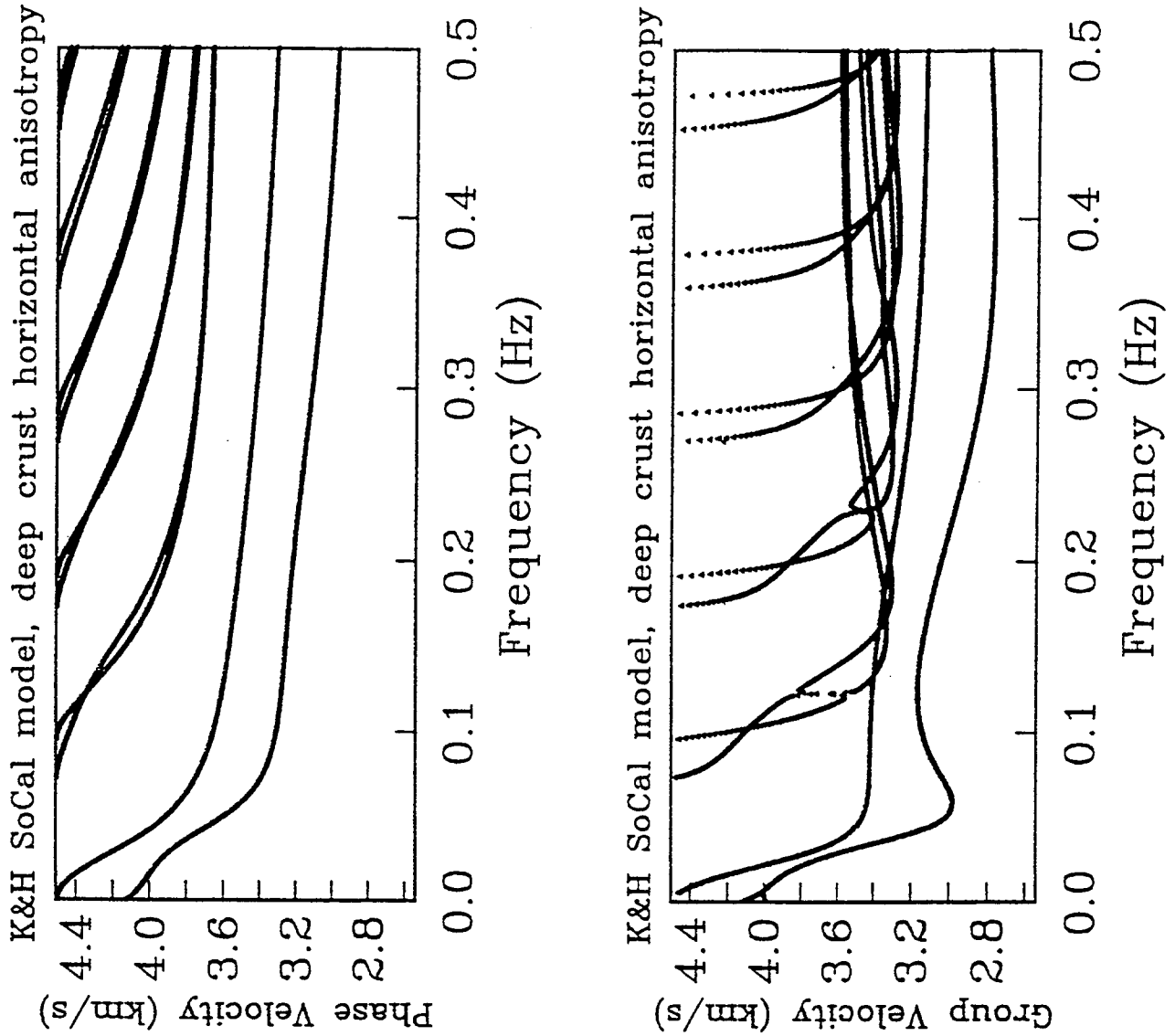

Figure 1. Dispersion curves for hybrid Love-Rayleigh surface waves in an anisotropic crustal waveguide. The velocity model is a modified form of the one-dimensional velocity model used to locate earthquakes in Southern California. Anisotropy with a horizontal axis of symmetry at 45° angle to the propagation is assumed, with 4% peak-to-peak variation in P-velocity and 2% peak-to-peak variation in S-velocity, both with $\sin 2\theta$ azimuthal dependence. The anisotropy is prescribed only in a 5-km thick layer at the base of the crust, consistent with the crustal extension common in the western US. The Love and Rayleigh dispersion curves tend to couple strongly where they cross in the phase-velocity graph, making "bridges" between pairs of group velocity curves. The eigenfunctions for these dispersion branches (not shown) exhibit significant mixing of Love and Rayleigh particle motion, even far from these crossing points.

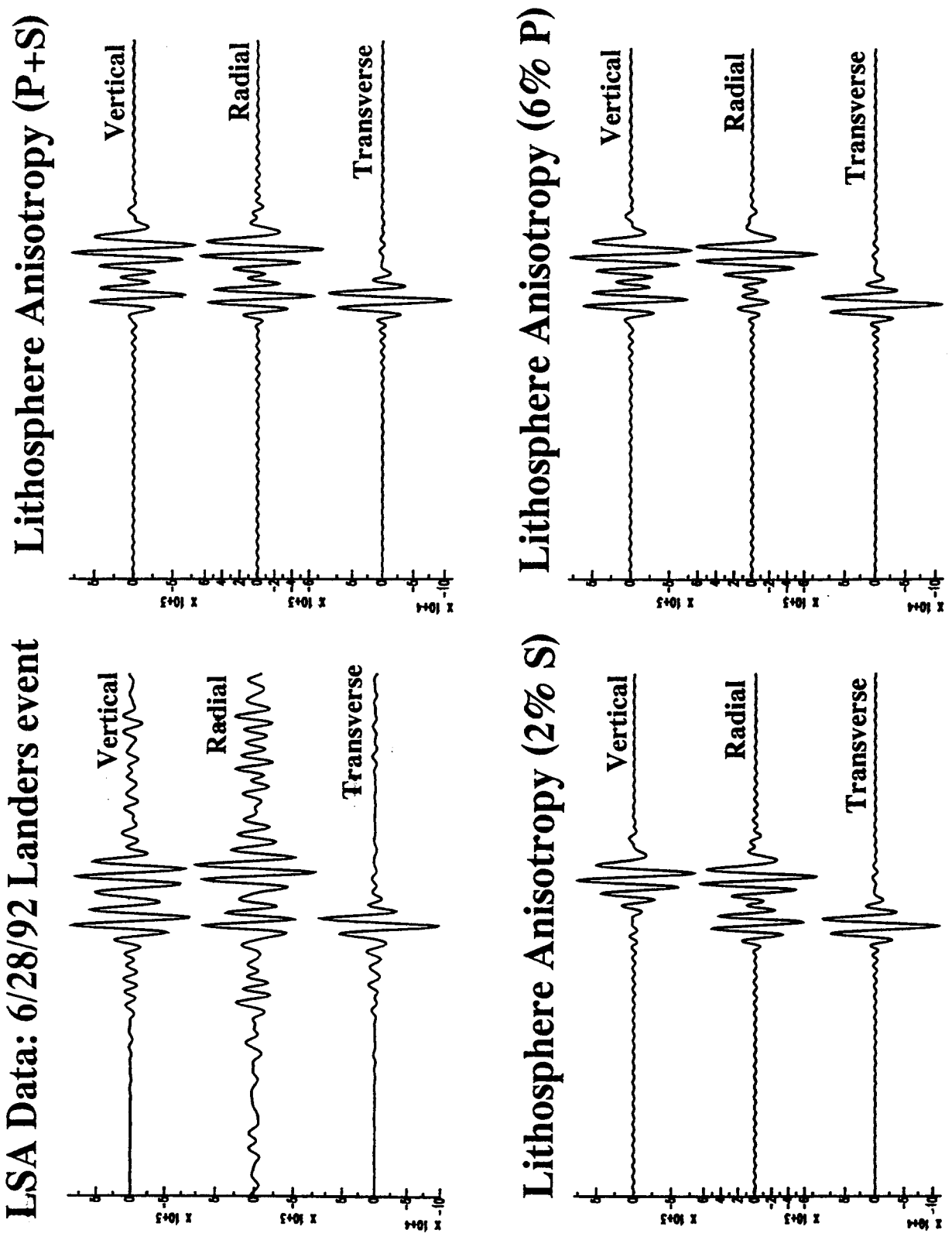

Figure 2. The upper right panel shows broadband data from 28 June 1992 Landers, California event, recorded at CDSN station LSA (Lhasa, Tibet). The lower right panel shows the coupled-mode-sum synthetics with only S wave (2%) anisotropy, with an east-west horizontal symmetry axis, at 100-300 km depth, consistent with lithospheric compression beneath the Tanggula Shan mountain range in southern Tibet. The lower left panel shows the synthetics with only P wave (6%) anisotropy. The upper left panel shows the synthetics combined with 6% P anisotropy and 2% S anisotropy.

range, which indicates lithospheric, perhaps crustal, scattering. Although rough isotropic lateral structure can scatter Love to Rayleigh motion, significant scattering usually involves a strong deflection of the wave. Anisotropic structure is a better model for forward scattering, as the spatial distortion of the stress-strain relation better couples the Love and Rayleigh particle-motion polarizations.

We have looked at seismic data recorded by Terrascope from Pacific earthquakes in a broad azimuthal range, to examine forward-scattering across the array. For the 24 May 1994 strike-slip earthquake in Taiwan (M_S=6.6, depth=33 km), surface waves intersect the California coastline at a low angle to the North-America/Pacific plate boundary, and so are susceptible to severe multipathing and scattering. At the inland station GSC (Goldstone, CA) the wavelet transform of the three components (vertical, radial, transverse) reveals significant radial-component energy for the Love wave, and transverse-component energy for the Rayleigh wave. A clear quasi-Love scattered wave follows the Love wave closely on the vertical component, in the period range 40-100 seconds. Wavelet polarization analysis of the GSC record (Figure 3) shows that, though long-period (> 100 sec) Love polarization is undisturbed, the intermediate-period polarization suffers refraction and some elliptical motion on the horizontals. The projection of correlated motion onto the radial-vertical plane shows low-amplitude elliptical motion, consistent with the quasi-Love wave's "Rayleigh" nature. The first pulse of Rayleigh energy is strongly refracted at intermediate frequencies, by roughly 45 degrees!

We have solved for polarized signals that are correlated network-wide using a singular value decomposition (SVD) of a matrix of complex-valued "wavelet coefficients," very much like the complex values of a standard discrete Fourier transform, or DFT. There are two aspects of this that differ from standard array-stacking techniques, and which justify the extra processing of the SVD. First, the SVD looks for a signal expressed as a linear combination of wavelet coefficients. Since these are complex valued, relative time shifts between stations can be accommodated by the algorithm as phase shifts in the wavelet coefficients. In principle, the SVD-decomposition could solve for the proper stacking velocity of a pulse, and could capture the non-plane-wave nature of a wave scattered within or close to the sensors. Similarly, the distortion of the wavefront across the seismic sensors can be captured by the SVD algorithm, which does not prescribe a uniform polarization at all stations. For Terrascope data, application of the SVD algorithm reveals that strong refraction of surface waves, usually attributed to the continent-ocean boundary, appears to occur most strongly inland of the Los Angeles Basin along the San Andreas Fault (Figure 4). Similarly, we observe that Love-to-Rayleigh scattered waves tend to be stronger for inland, relative to coastal, Terrascope stations. This suggest that, from the point of view of forward scattering, the strongest lateral gradients of material properties in the upper mantle beneath Southern California are associated with the plate boundary, not the coastline.

The following papers have been supported by this contract thusfar:

Yu, Y., J. Park & Wu, F., 1995. Mantle anisotropy beneath the Tibetan Plateau: evidence from long-period surface waves, *Phys. Earth and Planet. Int.*, , *87*, 231–246.

Lees, J., and J. Park, 1995. Multiple-taper spectral analysis: A standalone C-subroutine, *Computers and Geosciences, 21,* 199–236.

Park, J., 1995. Seismic wave propagation studies in the US: 1991-1994, US National Report to the IUGG, *Reviews of Geophysics Supplement, 33*, 335–340.

Lilly, J. and J. Park, 1995. Multiwavelet spectral and polarization analysis of seismic records.

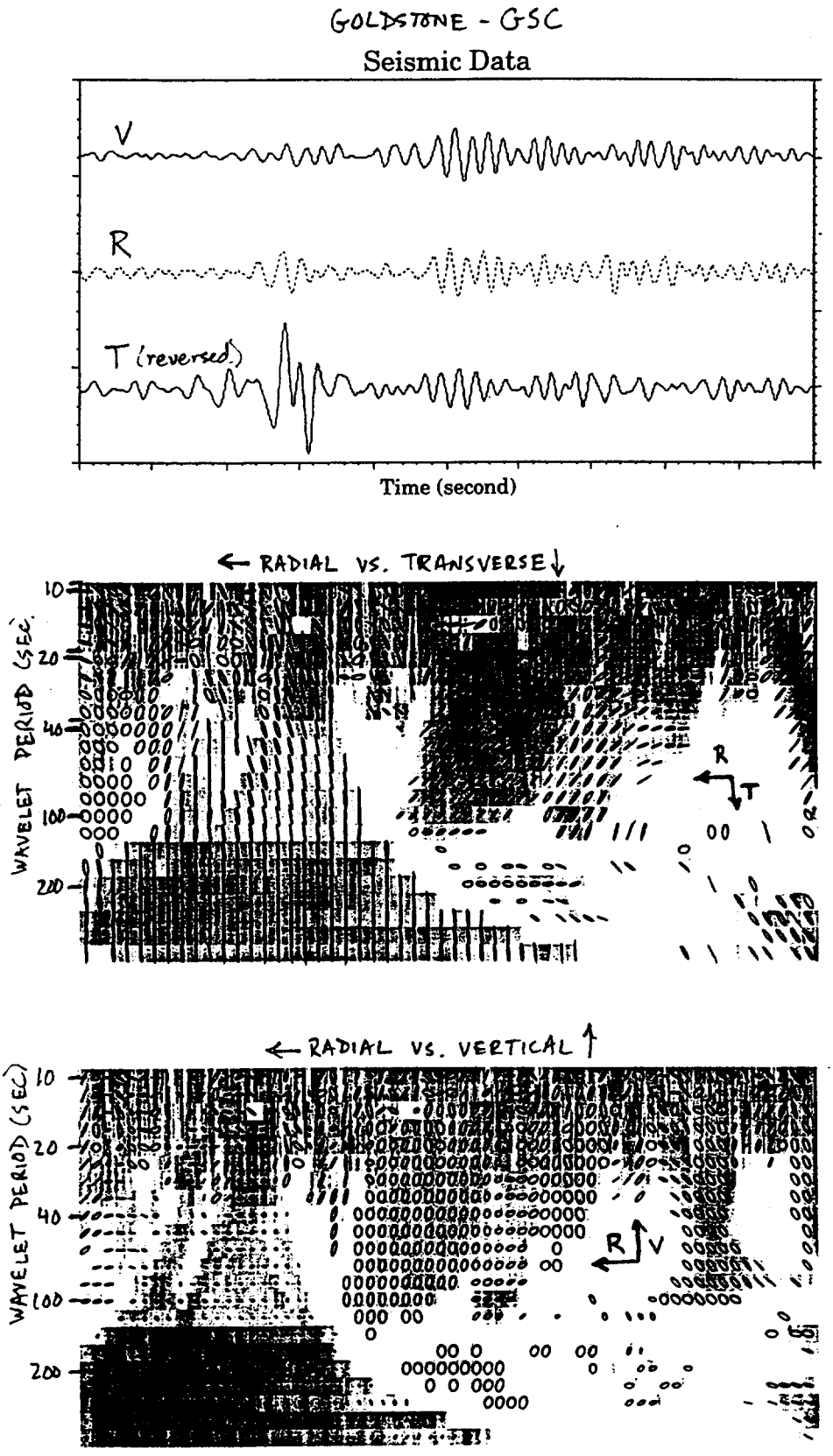

Figure 3. Multiwavelet polarization analysis of the 24 May 1994 Taiwan event recorded at GSC (Goldstone, CA). Our analysis uses three complex Slepian wavelets with $p = 2.5$, $p_c = 3.0$. The data is plotted in the upper panel, with horizontals rotated to radial and transverse directions. In the lower panels the normalized first singular value d_1 of the multiwavelet transform matrix M is shaded where it exceeds 90% confidence for nonrandomness. The center panel shows particle motion in the horizontal plane, with radial component oriented right-left, and the transverse component oriented up-down. The lower panel shows particle motion in the radial-vertical plane, with radial component oriented right-left, and the vertical component oriented up-down.

Propagation Direction of Rayleigh Wave

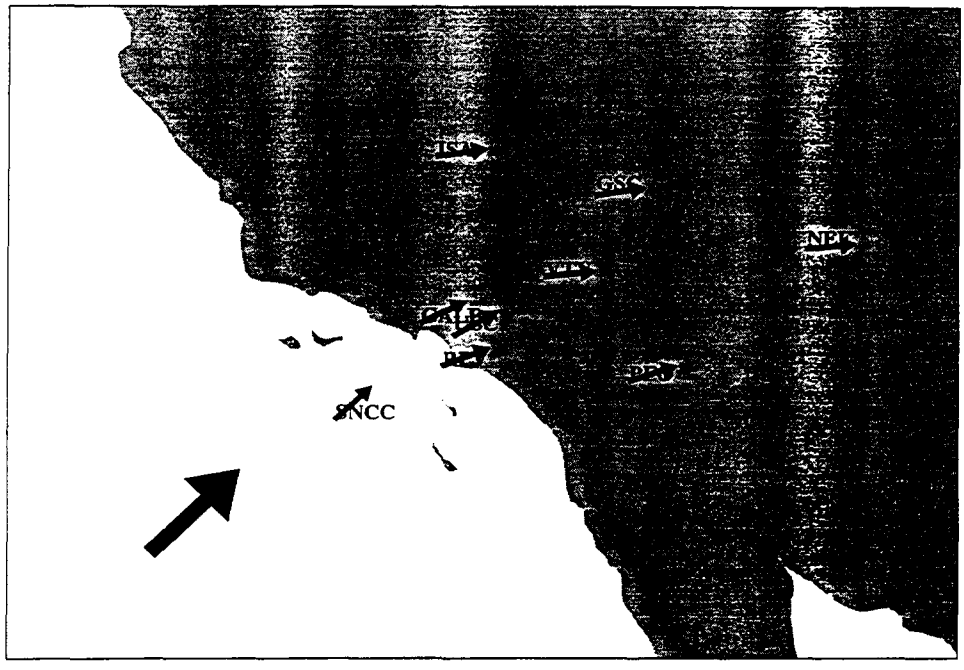

Propagation Direction of Love Wave

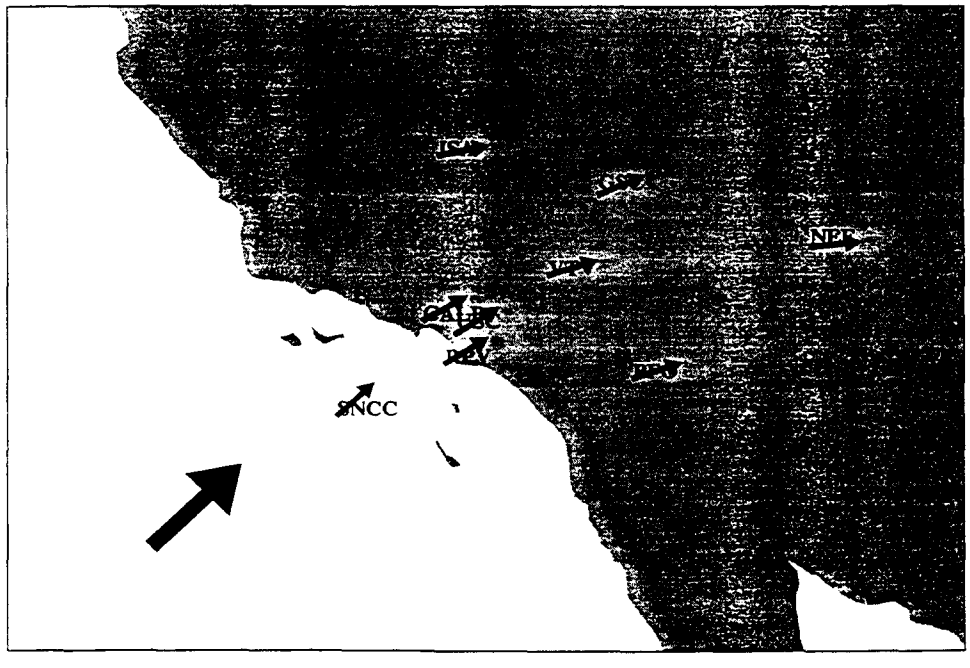

Figure 4. Wavelet polarization for 50 second surface waves across the Terrascope network in Southern California. The large arrow indicates the great-circle azimuth from the earthquake source, off the north island of New Zealand. Stations near the coast, including SNCC, RPV, CALB and USC, show little deflection of particle motion, but large deflections are apparent at inland stations ISA, GSC, NEF, VTV and PFO, all within or beyond the San Andreas deformation zone.

Geophys. J. Int., in press.

Su, L., and J. Park, Asymptotic path integral synthetics using the strong Born approximation, *Geophys. J. Int.*, in review.

RECOMMENDATIONS AND FUTURE PLANS

By the end of the year, we anticipate submitting manuscripts for publication in three areas. In particular, we plan to submit manuscripts 1) on the array-version of the multiple-wavelet transform, comparing crustal surface wave data from the Terrascope and Kyrghyzstan regional networks; 2) on the hybridization of Love and Rayleigh waves in 1-D anisotropic structures; 3) on the effect of receiver-side 1-D anisotropy, with an arbitrary symmetry axis, on upgoing body waves e.g. split shear waves and the shear-coupled PL wave.

Additional areas to explore:

1) We would like to apply the multiple-wavelet processing to an array with smaller aperture, like the broadband Pinon Flat experiment or the Geyocha array in Turkmenistan, and to go beyond a general study of wavefield properties to test the detection enhancement of wavelet-based techniques on surface waves at low signal-to-noise ratios.

2) We would like to examine the coupling of anisotropic crustal waveguide modes more fully, and compare theory with data in a more systematic manner. We anticipate using data from convergent-tectonic regions, like the broadband PASSCAL deployment in Tibet (we are familiar with this dataset, and have noted how Love-to-Rayleigh scattering becomes complex as periods decline from 100 to 50 seconds, as surface waves sample the mantle less and sample the crust more. Data from the broadband Kyrghyzstan network is also applicable in this context. We plan to test the behavior at some US stations where active-source seismic profiling has revealed a highly reflective lower crust e.g., within the Basin and Range Province. Some crustal seismologists have attributed this reflectivity to thin anisotropic layers, which would develop as a result of extensional thinning of the crust. It would be interesting to see if coupled-mode crustal surface waves can be used to confirm or deny this model.

REFERENCES

Backus, G. E., Possible forms of seismic anisotropy of the uppermost mantle under oceans, *J. Geophys. Res.*, *70*, 3429–3439, 1965.

Chen, X., 1993. A systematic and efficient method of computing normal modes for multilayered half-space, *Geophys. J. Int.*, *115*, 391–409.

Crampin, S., A review of the effects of anisotropic layering on the propagation of seismic waves, *Geophys. J. Roy. astron. Soc.*, *49*, 9–27, 1977.

Park, J., 1993. The sensitivity of seismic free oscillations to upper mantle anisotropy I: Zonal symmetry, *J. Geophys. Res.*, *98*, 19933-19949.

Shearer, P. M., and J. A. Orcutt, Compressional and shear wave anisotropy in the oceanic lithosphere - the Ngendie seismic refraction experiment, *Geophys. J. Roy. astron. Soc.*, *87*, 967–1003, 1986.